https://doi.org/10.5194/esurf-2021-4
Preprint. Discussion started: 10 February 2021

Stochastic alluvial fan and terrace formation triggered by a high-magnitude Holocene landslide in the Klados Gorge, Crete

Elena T. Bruni[1], Richard F. Ott[1], Vincenzo Picotti[1], Negar Haghipour[1, 2], Karl W. Wegmann[3, 4], Sean F. Gallen[5]*

[1] Department of Earth Sciences, ETH Zürich, Switzerland
[2] Laboratory of Ion Beam Physics, ETH Zürich, 8092 Zurich, Switzerland
[3] Department of Marine, Earth and Atmospheric Sciences, North Carolina State University, Raleigh, NC, USA
[4] Centre for Geospatial Analytics, North Carolina State University, Raleigh, NC, USA
[5] Department of Geosciences, Colorado State University, Colorado, USA

**Correspondence to*: Sean F. Gallen (sean.gallen@colostate.edu)
Elena T. Bruni (elena.bruni@erdw.ethz.ch

https://doi.org/10.5194/esurf-2021-4
Preprint. Discussion started: 10 February 2021

Earth Surface Dynamics Discussions

Abstract

Alluvial fan and terrace formation is traditionally interpreted as related to Quaternary climate oscillations under the backdrop of slow and steady tectonic activity. However, several recent studies challenge this conventional wisdom, showing that such landforms can evolve rapidly as a geomorphic system responds to catastrophic and stochastic events, like large magnitude mass-wasting. Here, we contribute to this topic through a detailed field and geochronological investigation of alluvial sequences in the Klados catchment in southwestern Crete, Greece. The Klados River catchment is characterised by well-preserved, alluvial terraces and a set of fans at the river mouth, which do not seem to fit the sediment capacity of a small catchment with a drainage area of ~ 11.5 km^2. Previous studies interpreted the formation of the deposits and their development to be of Pleistocene age and controlled by climate variations and the region's long-term tectonic activity. We find that the > 20m thick intermediate fan buries a paleoshoreline uplifted in AD 365 placing the depositional age of this unit firmly into the Late Holocene. This is supported by seven new radiocarbon dates that infer mid to late Holocene ages for the entire fan and terrace sequence. As sediment source, we identify a landslide scar at the head of the catchment. We document landslide deposits 100 m above the modern stream and utilise landslide runout modelling to reconstruct landslide volumes and validate our hypothesis. We find that a landslide volume of 0.0908 km^2 matches the observed distribution of landslide deposits and the landslide scar dimensions. We hypothesise that subsequent aggradation and incision cycles of the alluvial deposits are not linked to long-term tectonic uplift and climate variations but rather stochastic events such as mobilisation of sediment in large earthquakes, storm events, or blockage in the valley's narrow reaches. The Klados case study represents a model-environment for how stochastically-driven events can mimic climate-induced sedimentary archives, and how catchments can become ultrasensitive to external perturbations after catastrophic events.

https://doi.org/10.5194/esurf-2021-4
Preprint. Discussion started: 10 February 2021

Earth Surface Dynamics
Discussions
Open Access

1 Introduction

Alluvial fans and terraces are traditionally used as proxies for climate variations and tectonic activity. Within this view, their formation depends on climate-driven changes in the ratio of sediment supply and transport capacity superimposed on the long-term tectonic activity of the region (Bridgland et al., 2004; Bull, 1991; Merritts et al., 1994; Pazzaglia, 2013; Schumm, 1973). However, an increasing number of studies report that stochastic mechanisms such as landslides and autogenic fluctuation in river channel positions can also generate these landforms (Finnegan et al., 2014; Limaye and Lamb, 2016; Scherler et al., 2016). Such stochastically-generated deposits can resemble climate-forced alluvial terraces and fans in structure and sedimentology, possibly leading to erroneous interpretations of the processes responsible for their genesis. However, it is possible to distinguish between climatic and stochastic mechanisms for fluvial terrace and fan formation through careful field observation, precise geochronology, and comparisons to regional climate records (c.f., Scherler et al., 2016). Nevertheless, it remains unclear how rivers and river catchment systems react and recover from high-magnitude stochastic perturbations (i.e., a large landslide). Furthermore, little is known about how such catastrophic events alter earth surface dynamics, which might generate different responses to superimposed variations in climate and tectonics in affected and unaffected catchments. Here we contribute to the growing body of literature on the role of climatic versus stochastic mechanisms as a driver of rapid emplacement of fluvial landforms and the impacts of stochastic forcing on catchment-scale earth surface dynamics through the investigation of an exemplary alluvial fan system in a small, steep catchment on the southern coast of Crete, Greece (Fig. 1a).

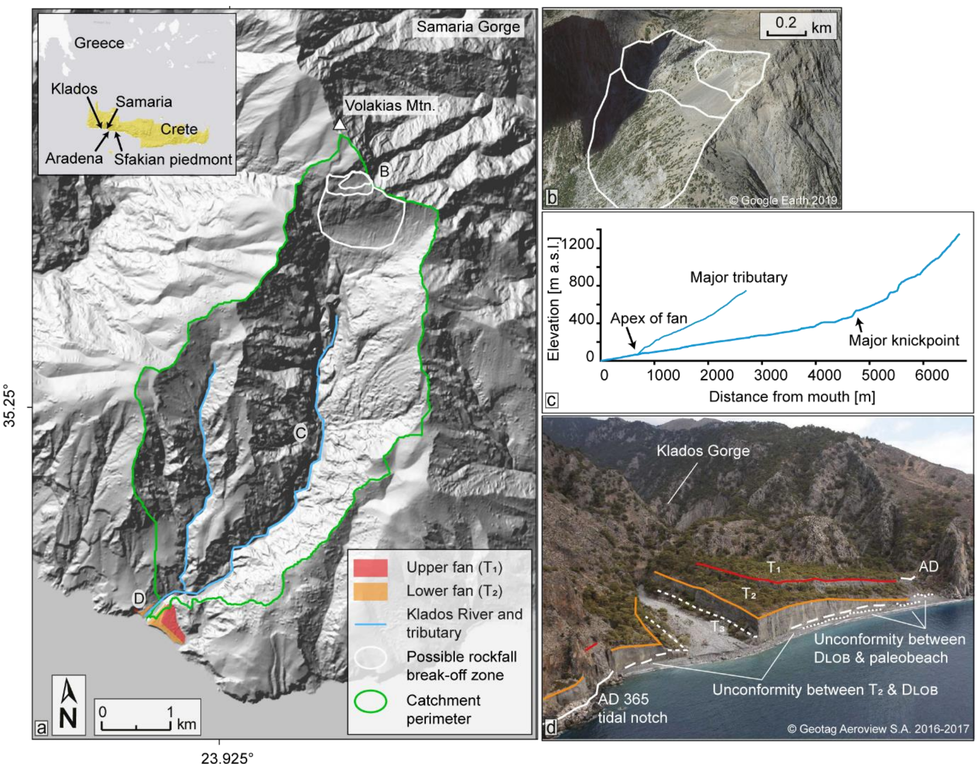

Figure 1: Overview of the Klados catchment and fan. (a) Hillshade of the Klados river catchment with the alluvial fan at its mouth (coloured). Note the steep planar surface at the head of the catchment, which we interpret as a rockfall failure plane. On it, the extents of the minimum, an intermediate, and the maximum rockfall areas are outlined as they are used in the landslide modelling in sect. 5.3. Inset overview of Klados catchment location on Crete, Greece, with the study area and other relevant locations indicated (ESRI, 2011). The hillshade was generated from the 5 m DEM of the Hellenic Cadastre SA. (b) Oblique perspective Google Earth view of the hypothesised failure plane(s) at the head of the catchment (outlined as in a). (c) River longitudinal profiles of the Klados River and its major tributary. (d) Oblique aerial photograph of the alluvial fans at the Klados catchment outlet (Geotag Aeroview, 2017). Highlighted are the different surfaces and unconformities discussed in the text.

Previous studies on Crete and elsewhere in the Mediterranean show that the construction of Quaternary alluvial terraces and fans are linked with climate fluctuations (Gallen et al., 2014; Macklin et al., 2010; Nemec and Postma, 1993; Pope et al., 2008; Wegmann, 2008). A key example comes from the alluvial fan system on the Sfakian piedmont of southern Crete ~30 km east of the Klados catchment. The Sfakia fan sequence was initially mapped and described by Nemec and Postma (1993) with subsequent detailed chronology developed by Pope et al. (2008), Ferrier and Pope (2012), and Pope et al. (2016) using luminescence dating and soil chronostratigraphy. From sedimentology, topographic surveys, soil redness indices, and chronometric dating, the Sfakian fans are interpreted as recording sediment deposition during colder and wetter glacial stages with little to no fan deposition during the intervening warm interglacial or interstadial periods (Pope et al., 2008, 2016). This result agrees with Gallen et al. (2014), who found that alluvial fans on the south-central coastline of Crete aggraded and prograded in response to both the increased catchment delivery of sediment and the lowering of the sea level (base level) during cold climate intervals. Similar conclusions were drawn by Wegmann (2008) and Macklin (2010), who found that active fan aggradation on Crete generally occurred during glacial stages. These examples illustrate that fan sedimentation occurred more or less in concert with Quaternary climate variability across western and southern Crete, similar to elsewhere in the Mediterranean (Benito et al., 2015; Macklin and Woodward, 2009; Thorndycraft and Benito, 2006; Zielhofer et al., 2008).

Most Cretan alluvial deposits share commonalities in stratigraphy, sedimentology, pedogenesis, and aggradational chronology. However, the alluvial fans and terraces preserved in the Klados Gorge are anomalous compared to nearby gorges, such as Samaria, and island-wide aggradational trends. The Klados River catchment drains the south flank of Volakis Mountain (2,200 m), which features a steep, 42° planar slope that dips southward off the mountain's upper flank (Fig. 1b). The stream incises metamorphosed Jurassic to Eocene Plattenkalk limestone (Creutzburg, 1977). Two large inset fans are present at the catchment mouth; they extend ~650 m along the beach between adjacent bedrock promontories (Fig. 1d). Wave action eroded the fan deposit toes, forming sea cliffs up to 30 m high. Each fan grades upstream into thick, well-preserved paired (valley-spanning) fill terraces (Fig. 2). Consequently, the volume of the Klados fan-terrace deposits is oversized relative to the relatively small catchment area (11.5 km^2), which is particularly evident when compared to deposits in the adjacent gorges with larger drainage areas. Furthermore, the alluvial fan-terrace deposits display little weathering and immature soil development, especially relative to the well-studied Late Pleistocene alluvial fan sequences preserved along the south coast of Crete (Gallen et al., 2014; Macklin et al., 2010; Nemec and Postma, 1993; Pope et al., 2008; Wegmann, 2008).

https://doi.org/10.5194/esurf-2021-4
Preprint. Discussion started: 10 February 2021

Earth Surface Dynamics
Discussions
Open Access

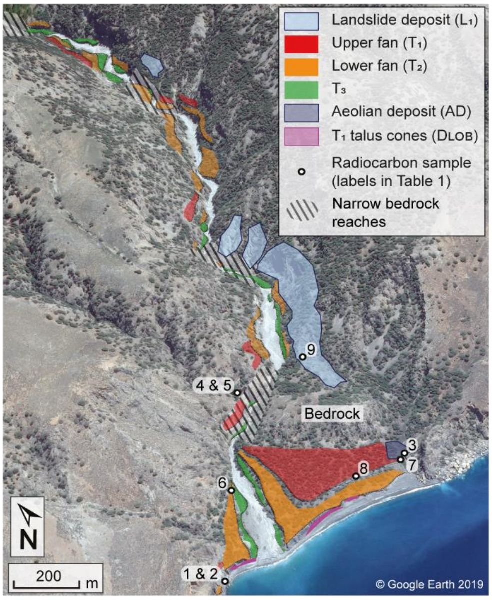

Figure 2: Overview of Quaternary deposits in the lower half of the Klados catchment. The numbers indicate the location of radiocarbon samples (labels correspond to Table 1). Note the inset fan surfaces at the outlet of the modern river mouth.

Previous research on the Klados alluvial sequence focused on the deposits close to the stream mouth. One study argues that alluvial deposits aggraded in the Holocene in response to short-term climate fluctuations, rapid uplift rate, and variations in sediment supply (Booth, 2010). In contrast, another study suggests that the fans are associated with Late Pleistocene climate-eustatic fluctuations and long-term tectonic uplift based on field observations and luminescence dating (Mouslopoulou et al., 2017). The correct interpretation of these exceptional deposits has important implications for understanding the role of climatic versus stochastic mechanisms on catchment-scale sediment transport, alluvial fan and terrace development, and the use of alluvial deposits as environmental archives in Crete and elsewhere.

Due to the unique appearance of the Klados sedimentary deposits, conflicting interpretations of their timing and genesis, and ambiguous geochronology, this study revisits the origin and evolution of alluvial deposits within and at the mouth of the Klados Gorge. The volumes of these deposits require an unusually high sediment supply for the catchment size. Through mapping and cross-cutting relationships, we show that a previously unidentified valley-filling landslide deposit - locally more than 100 m thick and in many locations encasing paleo-bedrock topography - is the source of sediment feeding the Klados alluvial fans. Relative and absolute dating place the deposition of the landslide and the construction of the alluvial fans and terraces firmly in the Holocene, contrary to previous luminescence ages. Our mapping, coupled with landslide runout modelling, suggests that a high-magnitude, catastrophic mass-wasting event in the catchment headwaters backfilled the valley. The rapid input of large quantities of sediment into the catchment provides an excellent opportunity to investigate how rivers respond to such catastrophic events.

https://doi.org/10.5194/esurf-2021-4
Preprint. Discussion started: 10 February 2021

2 Regional setting

Crete is in the forearc of the Hellenic subduction zone, where the African plate subducts beneath the Aegean microplate at a rate of ~35 mm a^{-1} (McClusky et al., 2000; Reilinger et al., 2006). The crust beneath Crete consists of a compressional nappe pile built during subduction in the mid-Cenozoic and exhumed in the Late Cenozoic (Fassoulas et al., 1994; van Hinsbergen and Meulenkamp, 2006). Miocene to Pliocene marine sediments in-filled extensional basins. These basins subsequently uplifted several 100s of meters and are now exposed above sea level on Crete (van Hinsbergen and Meulenkamp, 2006; Meulenkamp et al., 1994; Zachariasse et al., 2011). Quaternary paleoshorelines document ongoing uplift; some are now hundreds of meters above sea level (a.s.l.) (Angelier et al., 1982; Gallen et al., 2014; Ott et al., 2019b; Robertson et al., 2019; Strasser et al., 2011). Craggy cliffs interrupted by deeply-incised valleys and bedrock gorges characterise southwest Crete's coastal topography, where basin-average erosion rates are ~ 0.1 mm/a (Ott et al., 2019a).

The island lies above the most active seismic zone in the Mediterranean, and episodic Holocene uplift in western Crete associated with earthquakes occurs under the backdrop of slower steady rock uplift driven by deeper crustal processes (Gallen et al., 2014; Ott et al., 2019b; Pirazzoli et al., 1982; Shaw et al., 2008; Stiros, 2001). Evidence of large earthquakes comes from historical reports, archaeological excavations, tsunami deposits, and uplifted Holocene paleoshorelines (Ambraseys, 2009; Dominey-Howes et al., 1999; Pirazzoli et al., 1996; Shaw et al., 2008). The uplift of a Holocene paleoshoreline by as much as 9 m a.s.l. on the southwestern coast of Crete is often attributed to an unusually large earthquake (Mw 8.3–8.5) in AD 365 (Mouslopoulou et al., 2015; Shaw et al., 2008). This prominent paleoshoreline is observable along > 200 km of coastline in western Crete and provides a robust Late Holocene time marker. At the mouth of the Klados catchment, the tidal notch is at 6 m a.s.l. and is used as a relative age marker.

https://doi.org/10.5194/esurf-2021-4
Preprint. Discussion started: 10 February 2021

3 Field and laboratory methods

3.1 Field observations and spatial analysis

Field mapping was complemented by spatial analysis of digital elevation models (DEM) using ArcGIS v10.2 and TopoToolbox v2 (ESRI, 2011; Schwanghart and Scherler, 2014). The field mapping focused on stratigraphic and sedimentological characteristics of the Late Quaternary deposits, cross-cutting relationships, and the degree of soil formation that allowed for the classification of distinct geomorphic units (IUSS Working Group WRB, 2015). A 5 m DEM of the catchment, provided by the Hellenic Cadastre SA, was used to determine the longitudinal river profile and the heights of the terraces above the modern channel elevation. The DEM was also used to reconstruct the extent and volume of eroded Quaternary alluvial fill deposits. For this analysis, we used elevation data from mapped geomorphic units that exhibited little erosion to model a given deposit's pre-incision surface. These pre-incision surfaces were constructed via spline (regularised, weight = 0.1) interpolation in ArcGIS. To determine eroded volumes and the original extent of the deposits, we subtracted the modern DEM from the interpolated pre-incision surfaces. Subsequently, a reconstruction of the pre-deposition valley bedrock morphology was created by subtracting the thicknesses of individual deposits from the modern DEM.

3.2 Radiocarbon dating

3.2.1 Fossils

Two vermetid shells were sampled at 5 and 6 m a.s.l. to constrain the age of the uplifted tidal notch, presumed to be upheaved in the AD 365 earthquake. The samples were crushed, washed in 0.06% HCl, and infused with 85% phosphoric acid. After graphitisation of the released CO_2 in an AGE3 system (Wacker et al., 2010), the resulting ~ 1 mg of graphite was analysed by an Accelerator Mass Spectrometer (AMS). The standards used in the graphitisation step are 8.55–9.12 mg IAEA-C1 carbonate and 9.97–10.54 mg IAEA-C2 I Travertine carbonate. We also collected a terrestrial gastropod shell from the upper fan surface in reddish silt to constrain the minimum age of fan surface abandonment. The sample was prepared using standard methods, and DirectAMS conducted measurements. The radiocarbon ages are reported in fraction modern (fm) values and years (yrs.) with a 1 σ range.

3.2.2 Bulk sediment measurements

To constrain the timing of aggradation and incision of the deposits, we radiocarbon-dated bulk organic matter collected from six fine-grained lenses within the deposits. We decided against using luminescence dating because of the sparsity of quartz and feldspar in the local carbonate bedrock and the turbulent mode and the short distance of transport that may result in incomplete bleaching, especially of feldspar grains (Rhodes, 2011). The samples consist of 0.02 to 0.03% wt. % of total organic carbon. The samples were extracted, fumigated with HCl at 70 °C for three days, and neutralised using NaOH (McIntyre et al., 2017). Due to low TOC, we measured two gas target runs with ~ 80 mg of sample in the first and ~ 120 mg in the second. The samples have been corrected for constant contamination correction using shale (fm=0.018 and Swiss soil fm=1.06) with a Matlab code described in Haghipour et al. (2019). The radiocarbon ages are reported in fraction modern (fm) values and years (yrs.) with a 1 σ range.

https://doi.org/10.5194/esurf-2021-4
Preprint. Discussion started: 10 February 2021

3.3 Parameters used in the landslide modelling

To test the feasibility of the rockfall hypothesis, we utilised the DAN3D-Flex dynamic landslide runout model that allows an initial coherent phase of motion followed by the flow-like movement of the rock mass (Aaron et al., 2017). Several studies report successful model results for landslides when a Voellmy or frictional rheology is used as the basal rheology (Aaron and Hungr, 2016; Grämiger et al., 2016; Hungr, 1995; Nagelisen et al., 2015). The model requires input files containing the pre-failure surface combined with the topography of the sliding surface over which the slide flows ("path topography") and the vertical depth of the sliding mass at the initial position represented by the source material isolated from its surrounding ("source depth").

Input parameters of topography, sliding surface and volume were estimated and calculated based on the modern topography. We produced a DEM of the modern landscape without the Holocene deposits mapped in this study as the pre-landslide topography (DEMpre). For this, the thicknesses of all deposits were subtracted from the present-day topography, thus creating a rough minimum estimate of the valley's bedrock topography before the landslide event (Fig. S2). The thicknesses were assumed to correspond to the elevations of the terraces from the modern river bed. DEMpre was also used to estimate the volume of the initial landslide valley infill. For this, we interpolated a horizontal plane of constant elevation at the maximal elevation of the landslide deposit at 100 m and subsequently measured the vertical distance from this plane to the pre-landslide topography (DEMpre). This calculation provides an estimate of the volume necessary to reach the given plane of elevation, even though it neglects the effects of topographic obstruction by the narrow valley reaches. Additionally, we approximated the possible maximum and minimum volumes for the valley infill by varying the landslide deposit elevation by 20 m.

We calculated several scenarios for the initial amount of material that detached from the mountain face as a wedge failure and compared them to the volumes of the valley infills produced as described above. For this, we estimated the thickness of the pre-failure rock slab on the mountain-face scarp based on its friction angle and the extent of the modern planar surfaces. The best-fitting volumes between the valley infills and the wedges were subsequently used to approximate the rockfall's initial size and model the landslide runout.

https://doi.org/10.5194/esurf-2021-4
Preprint. Discussion started: 10 February 2021

4 Results

The Klados catchment contains three generations of alluvial infills (denoted as T_1, T_2, and T_3, from highest to lowest, respectively) extending from the river headwaters to the beach, where they terminate in large telescopic fans (Figs. 2, 3). The two upper alluvial infills (T_1 and T_2) form steep coastal cliffs separated from the sea by a 2-10 m wide cobble-pebble beach while the lower fill (T_3) grades into more recent fluvial gravels downstream. The Klados River incised into each of the alluvial deposits, forming terrace treads at ~ 50, 20, and 5 m above the modern channel, respectively. An additional deposit (L_1) is found as high as 100 m above the channel and has an irregular basal contact that fills in a paleo-bedrock topography. It does not grade into a fan, and its sedimentology is distinct from the alluvial deposits, suggesting formation by a different process.

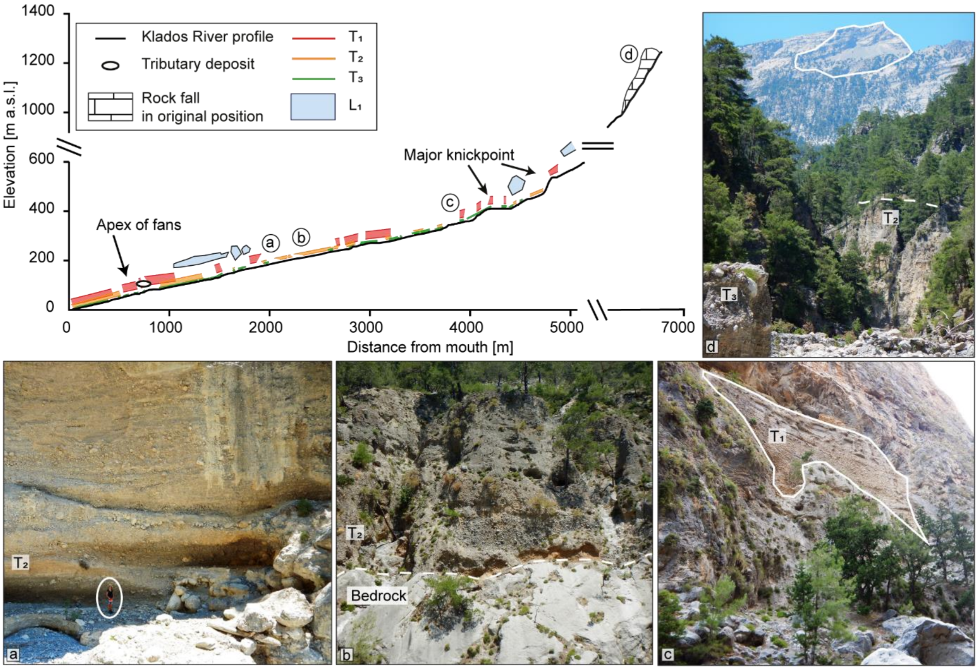

Figure 3: Klados River longitudinal profile. Both the top tread and the bottom contacts of the mapped infills can be traced from the headwaters to the sea, where they form the massive alluvial fans. The hypothesised position of the initial rockfall is indicated. (a) The valley is filled with thick (> 30 m) terraces (person for scale). (b) Contact between bedrock and T_2 valley infill. (c) The T_1 valley infill deposits are found up to 60 m above the modern river channel. (d) Distant view of the potential rockfall source on Volakias Mtn. (highlighted).

Deposits T_1 and T_2 cut and form buttress unconformities in various locations against the L_1 deposit, indicating that the alluvial deposits were emplaced after the deposition of L_1 (Figs. 3, 4a). Basal unconformities (i.e., straths) of the alluvial and L_1 deposits rarely crop out in the lower reaches but are increasingly visible upstream (Fig. 3). Nevertheless, we identified that T_2 unconformably overlies a paleo-beach deposit, the top of which lies at the same elevation as the AD 365 tidal notch that is cut into the limestone headlands on either side of the Klados valley (Figs. 1d, 4e). An Aeolian deposit locally tops the T_1 surface proximal to the seaward cliff. In addition to

https://doi.org/10.5194/esurf-2021-4
Preprint. Discussion started: 10 February 2021

these prominent deposits, we identified several smaller, more recent infills distributed over the catchment's lower reaches.

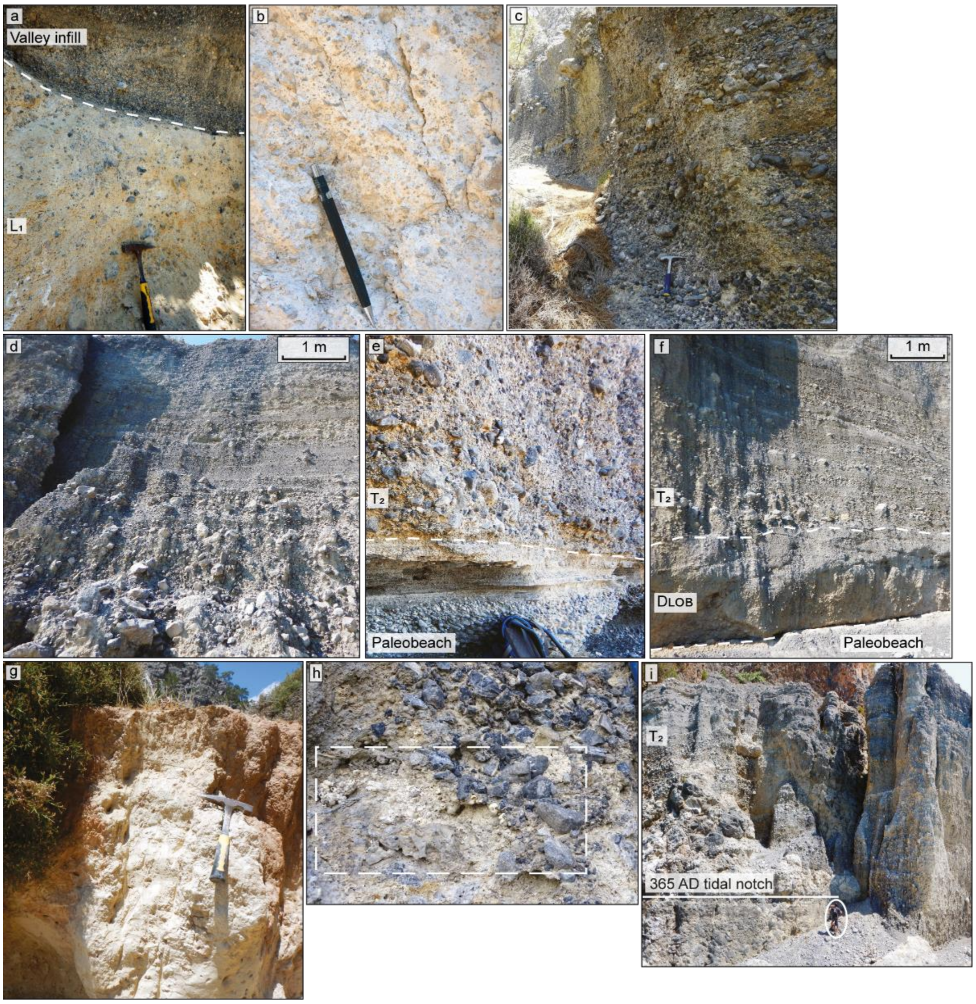

Figure 4: Images of the main deposits and their unconformities. (a) Unconformity between the landslide deposit (L_1) and one of the valley infills. (b) Typical appearance of the landslide deposit characterised by angular clasts floating in a fine matrix. (c) The top section of the upper fan (T_1) is characterised by cobble to pebble-dominated laminar sheet flow deposits. (d) T_2. Note grading from unsorted, subangular boulders and cobbles to a laminar deposit similar to (c). (e) The unconformable contact between the paleobeach and the lower fan (T_2) deposits. The paleobeach grades from discoidal cobbles to pebbles and sand from the beach berm facies deposition. (f) Paleobeach buried by D_{LOB} and T_2 close to the modern river channel. (g) Aeolian deposit from the eastern fan (T_1) surface. (h) Vermetid shells at radiocarbon sampling sites 1 & 2, growing within the uplifted tidal notch covered by angular fan deposits. (i) Same location as (h), highlighting the stratigraphic relationship between the tidal notch uplifted in AD 365 and T_2, which covers the notch (person for scale).

4.1 The Klados catchment infill units

At ~100 m above the modern channel, we locate a light-coloured, unsorted, and unconsolidated deposit (L_1) with matrix-supported, subangular clasts (Fig. 4a, b). No bedding or other flow indications, such as imbrication, sigmoidal structures, or layering, are preserved within the deposit (Fig. 4a, b). The L_1 deposit shares many similarities with rock avalanche deposits described elsewhere by Dufresne (2017), which is why we interpret the deposit's observable parts as the body facies of a landslide. The carapace and basal facies are not observable and may have been locally eroded or buried by stream and hillslope geomorphic processes following landslide deposition. The deposit is present along the gorge's walls up to the headwaters, where it locally backfills the pre-existing bedrock topography in paleo-tributaries.

The alluvial fill units (T_1, T_2, and T_3) each consist of a coastal fan and its equivalent terrace in the gorge. These units consist of unconsolidated, matrix-rich but grain-supported, subangular to subrounded carbonate boulder- to silt-sized clasts (Fig. 4c, d). At the outcrop-scale, the clasts exhibit a crude fining upward trend from a coarse, unsorted, angular to subangular, matrix-rich basal association of boulders, cobbles, and pebbles to meter-scale beds of moderately sorted cobbles, pebbles, and sand. This vertical variability is consistent for all the significant terraces such that the mean grain size and structure do not change between the infill deposits, except for occasional fine-grained lenses towards the top of the two highest coastal units (T_1 and T_2). The upper portions of the alluvial fill units are always layered and fluvially reworked, resembling sheet flow deposits (c.f., Blair and McPherson, 2015). Soils are weakly developed on all three alluvial fill units.

The T_1 basal layer is not exposed near the coast; however, the T_2 basal layers exposed adjacent to the modern channel show laterally changing grain sizes and structure. With increasing vertical distance to the channel thalweg, T_2 grades from a matrix-rich, unsorted association containing a variety of grain sizes (boulders to sand) to layers dominated by smaller clasts and increased sorting. The grain size distribution and structural observations suggest that the units' stratigraphically-lowest deposits correspond to debris flows buried by an increasing amount of braided river deposits.

A paleo-beach deposit at 6 m a.s.l. has similar sedimentology to the modern beach and consists of cemented, clast-supported layers of rounded, discoidal carbonate sand, pebbles, and small cobbles (Fig. 4e). Two units overlie the paleobeach, the T_2 basal debris flow in the west, and an intermediate deposit characterised by smaller grain sizes and lobate structures (D_{LOB}) in the east (Fig. 4f). D_{LOB} most likely consists of the talus cones formed during the erosion of the T_1 cliff before T_2 deposition.

The T_1 fan is locally topped by a discontinuously laminated, homogeneously reddish silty clay (unit AD; Figs. 2, 4g). It contains a few angular pebbles (~1 cm) and terrestrial snail shells. The material is interpreted as wind-transported sediment commonly found in the coastal areas of Crete. Deposition and preservation of this Aeolian deposit commenced after the abandonment of the T_1 surface during the incision phase. Thus, the T_1-AD unconformity and the radiocarbon measurements of the shells in the AD deposit constrain the onset of incision after T_1 aggradation.

https://doi.org/10.5194/esurf-2021-4
Preprint. Discussion started: 10 February 2021

4.2 Cross-cutting stratigraphic relationships reveal the relative sequence of events

Stratigraphic contacts between units provide us with a relative sequence of events and a possible timeframe for the individual aggradation and incision phases. Inset relationships and buttress unconformities allow for a relative chronology for L_1 and the alluvial deposits (T_1, T_2, and T_3). T_1 is inset into and forms a buttress unconformity with L_1 (Fig. 4a), and the same relationship exists between T_1 and T_2, and T_2 and T_3. These cross-cutting relationships show that the valley-filling units, arranged in age from oldest to youngest, are L_1, T_1, T_2, and T_3. Note that this sequence requires repeating episodes of valley-wide aggradation and incision. In the lower parts of the valley, incision cuts into pre-existing fill forming a buttress unconformity, while farther up valley incision persists through the pre-existing fill and into bedrock generates bedrock straths.

Along the coast, we observe other cross-cutting relationships relevant to the timing of T_1 and T_2 deposition. Firstly, the contact between T_1 and the Aeolian deposit (AD) represents the end of the T_1 aggradation phase and the onset of T_1 incision. The sharp, undisturbed contact points to a rapid shift from aggradation to T_1 surface abandonment. The radiocarbon ages of terrestrial snail shells from the Aeolian deposit provide maximum ages for fan surface abandonment. Secondly, angular pebbles of the T_2 infill cover the vermetids and sea urchins on the Late Holocene tidal notch (Fig. 4h). This observation demands that the paleo-sea level marker was carved before T_2 deposition. Finally, T_2 unconformably overlies the paleobeach deposit that is horizontally aligned with the tidal notch. These observations corroborate that the carving of the tidal notch and the formation of the paleobeach are connected, but also that the T_2 debris flows were deposited only later, after a temporal gap of unknown duration.

4.2.1 Upvalley trends of the alluvial infill deposits

Each valley infill was deposited in a separate aggradation event, followed by a phase of incision during which the river attempted to adjust its slope, eventually reaching and incising the bedrock in the valley's narrow reaches. The structure and sedimentology of the infill terrace deposits change vertically from unsorted debris flows at the bottom to layered sheet flows and regular riverine deposits at the terrace tread. These trends are consistent along the river channel from the mouth to the headwaters. Thus, the initiation (trigger), transport, and deposition processes were very similar during each aggradation phase, while the onset of incision between aggradation intervals acted as the turning point that allowed the system to repeat the cycle. However, the elevation at which we find the terraces increases upstream because we find straths and the bottom contacts of the infills in the headwaters, both of which are generally absent in the lower reaches. We can utilise these bottom contacts to reconstruct the then-active river channel, which steepens upstream relative to the modern profile. This illustrates that the headwater reaches were subjected to greater incision relative to the outlet due to sediment overload and that the subsequent aggradation events were fed from the landslide deposits upstream. This resulted in a transfer of sediment from the headwaters to the river's mouth and an increasing adjustment of the channel slope.

4.3 Radiocarbon dating of shells

The radiocarbon dating of vermetid shells constrains the timing of uplift for the paleobeach and bioerosional notch. The ages are reported in years (yrs.) and fraction modern (fm) (Table 1). The samples, collected at and below the notch (Fig. 2), yielded ages of 2,672 ± 24 yrs. and 2,397 ± 25 yrs. for the uplift, respectively. These ages are older than the inferred 365 AD (c. 1,600 yrs.) age of uplift. The difference might be caused by the

https://doi.org/10.5194/esurf-2021-4
Preprint. Discussion started: 10 February 2021

Earth Surface Dynamics Discussions

organisms' death before the uplift due either to burial by prograding fans or natural causes. A terrestrial gastropod shell collected from the AD deposit capping T_1 yielded an age of 3,952 ± 24 yrs., thereby constraining the cessation of T_1 aggradation.

Table 1: Radiocarbon measurements from the Klados catchment. Results are reported in fraction modern (fm) and years (yrs.).

Label	ETH number	Deposit	Sample type	Coordinates	Fraction modern ± error absolute	^{14}C age (1 σ) ± error (yrs.)
1	82442.1.1	Tidal notch	Vermetid carbonate shells	35.2295 N 23.9093 E	0.717 ± 0.00213	2,672 ± 24
2	85020.1.1	Tidal notch			0.742 ± 0.00234	2,397 ± 25
3		Aeolian deposit (AD)	Terrestrial snail	35.2366 N 23.9159 E	n/a	3,952 ± 24
4	94494.1.1 87102.1.1	Tributary (TD_1)	Bulk sediment	35.2320 N 23.9155 E	0.573 ± 0.00690 0.711 ± 0.00695	4,820 ± 556 2,696 ± 369
5	94495.1.1 87100.1.1	Tributary (TD_2)	Bulk sediment	35.2320 N 23.9155 E	0.566 ± 0.00690 0.663 ± 0.00657	4,820 ± 379 3,389 ± 587
6	94493.1.1	Lower fan (T_2)	Bulk sediment	35.2308 N 23.9125 E	0.583 ± 0.00680	4,793 ± 826
7	94491.1.1 87103.1.1	Upper fan (T_1)	Bulk sediment	35.2266 N 23.9156 E	0.531 ± 0.00650 0.613 ± 0.00714	5,788 ± 874 4304 ± 903
8	87103.1.1	Upper fan (T_1)	Bulk sediment	35.2275 N 23.9140 E	0.579 ± 0.00602	5,131 ± 1,342
9	94496.1.1 87098.1.1	Landslide (L_1)	Bulk sediment	35.2309 N 23.9186 E	0.728 ± 0.00740 0.671 ± 0.00737	2,476 ± 351 3294 ± 831

4.4 Radiocarbon dating of alluvial infill deposits

Sedimentation ages were constrained by bulk radiocarbon dating, and are reported in ages (yrs.). The corresponding fraction modern (fm) values are specified in Table 1 and Fig. 5. For the alluvial deposits, samples were collected from fine-grained slack-water lenses at the top of each deposit (Fig. 2). The T_1 samples returned ages of 5,788 ± 874, 4304 ± 903, and 5,131 ± 1,342 yrs. The large uncertainty in the second date is caused by the low carbon content in the sample, and thus, the date needs to be interpreted with care. Due to the inaccessibility of fine-grained lenses on the seaward cliff of the T_2 deposit, samples were not collected. However, a sample collected from just below the tread and close to the apex of the T_2 fan yielded an age of 4,793 ± 826 yrs. Two samples ($TD_{1\ \&\ 2}$) from the fine-grained deposit at the confluence of the major tributary and the Klados River yielded 4,820 ± 556 and 2,696 ± 369 yrs., and 4,820 ± 379 and 3,389 ± 587 yrs., respectively. These ages confirm that at least one of the valley infills reached 40 m elevation upstream of the fan apex and blocked the tributary channel. The landslide deposit (L_1) dates to 2,476 ± 351 and 3,294 ± 831 yrs.

https://doi.org/10.5194/esurf-2021-4
Preprint. Discussion started: 10 February 2021

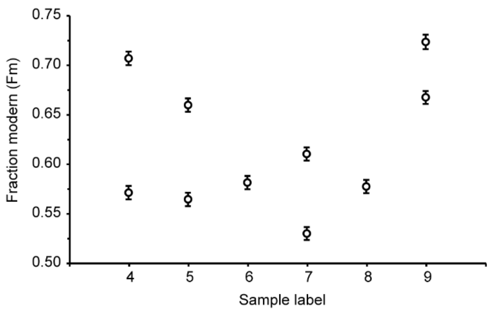

Figure 5: Fraction modern (fm) radiocarbon data of bulk sediment samples from the major deposits. Detailed information on the measurement is reported in Table 1. The data are presented with an absolute error. Sample labels 4 & 5= $TD_{1\,\&\,2}$, 6 = T_2, 7 & 8 = T_1, 9 = L_1.

The radiocarbon data presented here demonstrate that the Klados sedimentary deposits' deposition occurred during the mid-to-late Holocene. However, the order of some of the resulting ages is inconsistent with the relative sequence of events demanded by observed cross-cutting relationships. This mismatch is likely due to the admixture of organic carbon from different sources and the finite amount of measurable material recoverable from the samples. We discuss these sources of uncertainty in detail in the discussion below and base our further interpretations on the uncalibrated radiocarbon ages (yrs., 1 σ).

4.5 Volumes of rockfall and valley infill

The thicknesses of the potential source area rockfall slabs were estimated based on friction angles and the extent of the planar surfaces on Volakias Mtn. at the head of the Klados catchment (visualised in Fig. 6). The calculation resulted in six downward converging wedges between 2.8 x 10^{-4} and 3.82 km^3 (Table 2). The estimated volume of the valley infill, calculated as described above, is between 9.37 x 10^{-3} and 3.05 x 10^{-2} km^3 (Fig. 6). These values overlap with intermediate estimates for the rockfall slabs. The volumes in the best-fit landslide runout model lie within the range of our upper-intermediate wedge volumes and values reported for similar size events in previous studies (USGS, 2016). Thus, we expect volume estimates to be relatively robust.

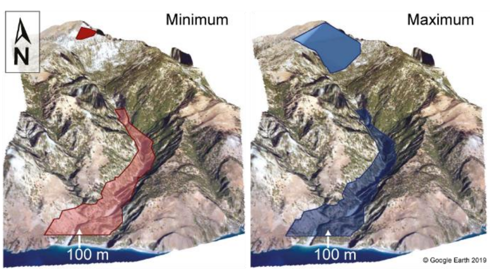

Figure 6: Visualisation of the minimum and maximum rockfall volume as calculated for the dynamic landslide runout model, and the highest possible reference plane inferred from the location of the highest mapped deposits during field observations (100 m above the modern river channel).

https://doi.org/10.5194/esurf-2021-4
Preprint. Discussion started: 10 February 2021

Earth Surface Dynamics Discussions Open Access EGU

Table 2: The maximum and minimum volume estimations for the rockfall, the valley infill, and the fan material. We calculated six downward-converging wedges of different volumes for the initial rockfall volume, whose intermediate values were fit for the landslide runout modelling.

	Minimum [km^3]	Maximum [km^3]	Intermediate [km^3]
Rock fall (wedges)	0.00028	3.82	0.8335 0.0223 0.00908 0.000918
Valley infill (landslide)	0.00937	0.0305	
Fans alone	0.00053	0.00115	

5 Discussion

5.1 Timing of the Klados catchment stratigraphy from relative and absolute dating

The agreement between our field observations and radiocarbon geochronology strongly supports a Holocene age for the alluvial infills in the Klados catchment. Despite their large uncertainties, all the radiocarbon measurements are Holocene and are mostly consistent with the observed cross-cutting field relationships. Even without the radiocarbon data, the following series of observations indicate geologically recent emplacement of the Klados alluvial fill units. Firstly, the buttress unconformity between the T_2 and the 365 AD paleoshoreline requires a post-AD 365 deposition of T_2. Secondly, the immature soils developed on T_1 and T_2 surfaces are inconsistent with the well-developed Bk and Bt horizons on Pleistocene alluvial fans with similar parent rock source areas (Gallen et al., 2014; Pope et al., 2008). Thirdly, the slopes of the T_1 and T_2 surfaces match the modern channel slope in the lower reaches, suggesting that the paleoriver prograded to a base level similar to the modern sea level. Finally, the morphology of the coastal cliff on T_1 and T_2 is similarly sharp (Fig. 1D; also see Fig. 4a of Mouslopoulou et al. (2017)). Given that both infills are unconsolidated sediment, one would expect relatively rapid diffusion and rounding of the paleo-sea cliff as noted along scarps produced by fault rupture (Nash, 1980) in similar sedimentary deposits.

The uncertainty on the relative age control on the landslide deposit (L_1) does not require a Holocene emplacement. However, due to this deposit's highly erodible nature, it is unlikely to persist in this landscape for an extended period, and soil development on this deposit is relatively immature. These findings, coupled with the Holocene bulk radiocarbon ages from the L_1 deposit, lead us to conclude that the landslide deposit is also Holocene.

Our radiocarbon ages are exclusively Holocene, but bulk radiocarbon measurements will introduce uncertainties to the chronology. Sources of error are diverse and closely related to environmental variables. At Klados, a decrease in measured age relative to real age most likely originates from the secondary incorporation of recent organic matter, while the inclusion of radiocarbon-dead bedrock carbonates causes an overestimation. Both of these sources of error are minimised in our approach. On the one hand, recent organic matter is often associated with large grain size fractions (c.f., Rothacker et al., 2013) and is easily avoided during sample collection and preparation. Conversely, the potential of sample age overestimation is minimised by fumigating the samples before measurement. This step ensures the substantial removal of inorganic carbonate. An uncertainty unrelated

https://doi.org/10.5194/esurf-2021-4
Preprint. Discussion started: 10 February 2021

to the environment is introduced by the low TOC and can result in smaller sample sizes prepared for the bulk radiocarbon measurement, which were affected with larger uncertainties after corrections for processing blanks and standards (Ruff et al., 2010). Nevertheless, empirical studies show that samples that contain a mixture of young and old carbon may overestimate the age of a deposit by 500–2000 years (Grimm et al., 2009; Rothacker et al., 2013). We recognise that the bulk sediment dating results contain inherent uncertainties and express reference timeframes rather than absolute ages for the processes due to a possible overestimation of the age.

Our Holocene radiocarbon ages complement field observations and provide additional age control. The deposition order obtained from the radiocarbon dating agrees with the sequence of events established in the field. The valley infill T_1 predates T_2, which is approximately the same age as the main tributary's slackwater deposits. The only outlier to the sequence is L_1. However, the clear stratigraphic relationship between L_1 and the other deposits overrules the radiocarbon dating. The most likely cause for the unlikely radiocarbon age is the introduction of younger organic matter after L_1 deposition by erosional processes, water movement, or bacterial activity. Consequently, both radiocarbon age dating and field observations imply the geologically recent deposition of the Klados stratigraphic sequence. Both the bulk sediment radiocarbon ages and the radiocarbon ages from shells are consistent with a Holocene age for all deposits. The cross-cutting relationships allow for a precise relative chronology of events during a relatively short amount of time.

The Holocene age for the Klados alluvial deposit sequence proposed here differs significantly from previous dating results by IRSL on feldspar (Mouslopoulou et al., 2017), which resulted in consistent Pleistocene ages for the infills (29-50 kyrs BP). However, the field observations and cross-cutting relationships demonstrate that these deposits are Holocene, supported by our radiocarbon analyses. The anomalously old luminescence ages reported by Mouslopoulou et al., (2017) are likely biased due to incomplete bleaching caused by the turbulent mode of transport and potentially the admixture of unbleached feldspars released from the carbonate pebbles during the acid treatment of the samples (Rhodes, 2011). The broad age distributions of Mouslopoulou et al., (2017) are likely indicative of a mix of bleached and unbleached grains resulting in late Pleistocene ages for both fan units. The local geological units are carbonates, so the source of the feldspar used for IRSL dating remains unclear (Creutzburg, 1977; Rhodes, 2011). Furthermore, the Pleistocene luminescence ages are difficult to reconcile in the context of similarly immature soil development and similarly crisp cliff morphology among deposits that are reported as greater than 30 kyrs old with ~10 kyrs separating the emplacement of each unit. For these reasons, we thus consider the IRSL dates from Klados as biased and not representative of the accurate depositional ages of the alluvial fans. Instead, the Klados alluvial fill deposits' Holocene age proves a more straightforward and more reasonable explanation for our data and field observations.

An important implication of the finding of Holocene ages for the stratigraphic units in the Klados catchment is that within short periods the catchment alternates between phases of valley-wide aggradation followed by intervals of rapid incision through the valley fill and into the bedrock in the upper portions of the catchment. This stratigraphic history is distinct relative to adjacent catchments that record slower and steadier aggradation and incision histories (Pope et al., 2008, 2016). This evidence indicates that local and unique processes in Klados are responsible for high-frequency pulses of aggradation and incision. We hypothesise that the large landslide deposit

https://doi.org/10.5194/esurf-2021-4
Preprint. Discussion started: 10 February 2021

(L_1), the oldest unit identified in the catchment, is the sediment source for the younger, inset alluvial fans, which is supported by our volume reconstructions and is in large part responsible for the unique stratigraphy and geomorphic evolution of Klados. We explore this hypothesis in detail below.

5.2 A rockfall source for Holocene deposits in the Klados catchment

Most of the adjacent gorges have alluvial infills, but these do not reach the thickness of the Klados deposits, and to date, only one other case study shows thick Holocene deposits. These are reported in the Aradena Gorge 10 km west of Hora Sfakia, where alluvial terraces up to 14 m above the modern channel bed are preserved (Maas and Macklin, 2002). They aggraded upstream from channel reaches temporarily blocked by landslide deposits and were incised in the next high-intensity discharge event. The authors dated the deposits to the last 200 years using lichenometry and dendrochronology preserved (Maas and Macklin, 2002). Even though the Aradena Gorge's deposits only span the last 200 yrs., the over-proportionate amount of sediment in the system and the rapid aggradation and incision rates recall the situation in the Klados Gorge where the large amounts of sediment are without an apparent source, and up to 30 m thick deposits of T_2 aggraded post AD 365. Moreover, the alternating narrow and wide sections in the Klados Gorge (Fig. 2) are prone to blockage, which may control sediment distribution and terrace genesis in a fashion similar to that reported by Maas and Macklin (2002). Both the Klados and the Aradena River deposits require rapid sedimentation rates beyond what is commonly reported, and the only possible explanations require local, isolated sources of sediment.

To elevate the sedimentation rates in the Klados Gorge, but not in adjacent gorges, and to enable the aggradation of such large volumes so quickly, an extraordinary but spatially limited sediment input is required. We hypothesise that a massive rockfall in the headwaters of the Klados River provided the necessary amount of loose sediment and the impetus for aggradation and incision. The rockfall hypothesis is the most straightforward option because the Klados catchment's hillslopes are supply-limited, mantled by only a thin layer of regolith. Furthermore, cosmogenically-derived erosion rates from nearby catchments in comparable rock-types suggest erosion rates on the order of ~0.1 mm yr^{-1} (Ott et al., 2019a), which is too low to generate the observed volume of detritus over Holocene timescales. Moreover, its unconsolidated state makes a landslide the ideal source material.

5.3 Landslide runout modelling supports the hypothesis of landslide sediment origin

Field observations document the presence of landslide deposits scattered throughout the valley. The spatial extent and sedimentology of this deposit are consistent with the pulverised remnants of a high-magnitude rockfall. The likely source for this rockfall is the cliff face at the headwaters of the Klados catchment (Figs. 1a, b, 3d). This cliff has overhanging rock bands that are diagnostic of recent rockfall events (Fig. 3d). Below these overhanging features, a steep (> 35°) planar bedrock slope abruptly terminates at the Klados catchment floor (Fig. 1a, b). We hypothesise that a large rock mass detached from the upper portion of this mountainside, dropped to the catchment floor, and pulverised upon impact, backfilling the paleo-valley. We envision a process similar to large rock falls with extended drop heights that have been observed in places like Yosemite Valley, CA (Wieczorek et al., 2000). The best-fit simulated runout for the landslide was obtained after multiple runs using inputs as defined in Table 3. Still images extracted from the model runout show the landslide's position and extent at selected time intervals (Fig. 7, Golden Software (2018)). The DAN3D-Flex model allows for an initial stage in which the rockfall slides

https://doi.org/10.5194/esurf-2021-4
Preprint. Discussion started: 10 February 2021

as a single, coherent mass (Aaron and Hungr, 2016). We constrained this gravitational movement to 30 seconds, after which the rockfall reaches the bottom of the sliding plane, hits the valley floor, and disintegrates (Fig. 7b). The rheology controlling flow behaviour changes upon impact from rigid body frictional to Voellmy-rheology controlled granular flow, consistent with our hypothesis that the rock mass pulverised upon impact with the valley floor. At about 45 seconds after initiation, the landslide reaches the sharp bend in the valley, slows down, and bulks up by the vertical concentration of the mass in the head of the landslide (Fig. 7c). After 60 seconds, the landslide is obstructed by the cliff in the centre of the modern fan structure (Fig. 7d). The modelled failure mass bulges up and overflows the cliff (Fig. 7e, f). No high-resolution bathymetry data were available, which precluded offshore runout modelling. The average deposit thickness is highest in the centre of the channel and decreases with distance to the impact site because entrainment was forbidden while the loss of material by deposition was implemented in the model. The averaged thicknesses at the final model time-step correspond well with the elevations of the landslide deposit in the field of ~ 100 m. From the model outputs, the narrow sections of the valley did not obstruct the flow too much, which suggests an even distribution of the landslide material.

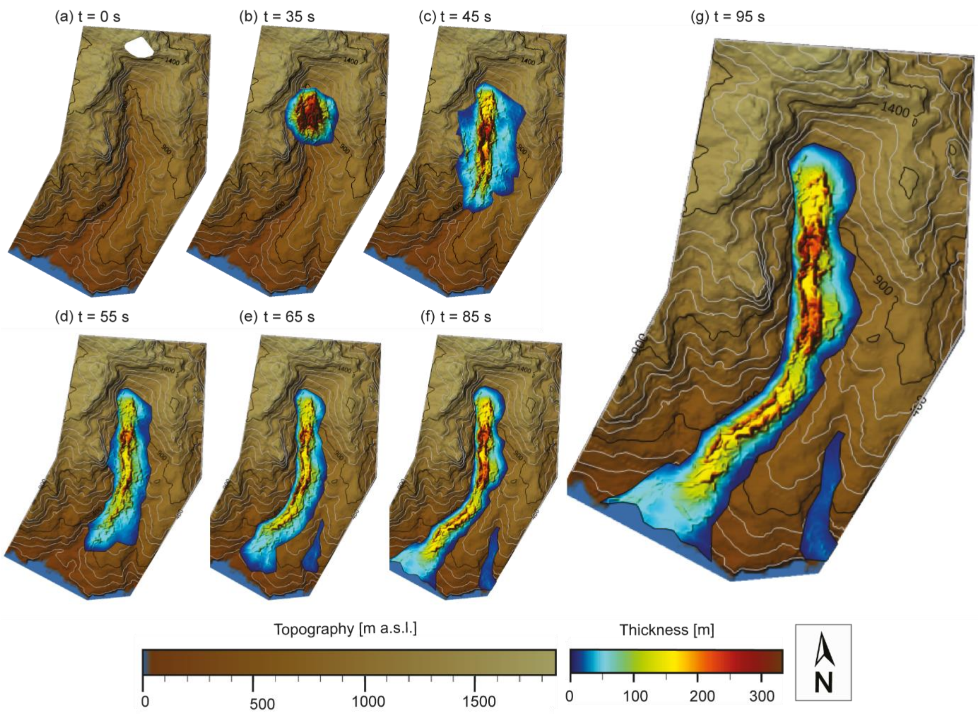

Figure 7: Time slices from the landslide runout modelling with an intermediate rockfall volume (0.0908 km³). The rockfall moved as an intact block from the mountainside, but partly pulverised and liquefied upon impact with the valley floor. It filled the valley in a ground-based landslide and a cloud of dust. The landslide eventually reached the sea, leaving scattered deposits up to 200 m thickness in the centre of the valley. No major blockage is shown in the narrow valley reaches. The model indicates that part of the landslide crossed into the adjacent valley, but this part of the coastline was not investigated during fieldwork.

https://doi.org/10.5194/esurf-2021-4
Preprint. Discussion started: 10 February 2021

Earth Surface Dynamics Discussions

Table 3: Parameters for the five best-fit landslide runout models. The quality of correlation between the model and field observations decreases with increasing numbering (1-5).

Quality of correlation	**1**	**2**	**3**	**4**	**5**
Rheology	Voellmy	Voellmy	Frictional	Frictional	Frictional
Input volume [km^3]	0.0908	3.34	0.00908	3.82	0.00908
No of particles	2000	2000	2000	2000	2000
Time steps [s]	0.1	0.1	0.1	0.1	0.1
Velocity smoothing coefficient	0.02	0.02	0.02	0.02	0.02
Stiffness coefficient	200	200	200	200	200
Rigid behaviour time [s]	30	30	10	10	30
Unit weight [kN m^{-3}]	21.5	21.5	20	20	20
Internal friction angle	35	35	15	15	20
Friction coefficient	0.2	0.2	0	0	0
Viscosity [kPa s]	0	0	–	–	-, 1000, -
Turbulence coefficient [m s^{-2}]	500	500	0	0	0, 500,0
Internal friction angle	35	35	35	35	35
Maximum slide velocity [m s^{-1}]	213.7	308.873	658.5	770.415	246.3
Travel time [s]	99.8	107.6	85.4	94.2	34.4

The best-fit runout model agrees particularly well with our field observations of landslide deposit thickness and the resulting valley infill's extent. The model results show that the material moved through the valley and was deposited at a sufficient thickness and elevation above the paleochannel to explain the deposits we identified in the field. Furthermore, the modelled flow rheology is consistent with the observed deposit sedimentology. The dominance of fine grains can be explained by the initial rockfall evolving into two modes of transport upon impact with the valley floor. If correct, the impact with the valley floor transformed the rockfall into a partly "liquefied" landslide due to air inclusion and abrasive grain interaction, but also a wind-blast driven sand-cloud which reached several hundred meters elevation (cf. Wieczorek et al., (2000)). Fluvial reworking mainly affected the landslide's coarse-grained parts in the valley while the finer-grained portion remained on the catchment walls. Nevertheless, the two modes of transport might explain the high amount of fine material in the subsequent alluvial deposits, as they were sourced from both of the landslide deposit types. Our model offers a first insight into the initial rockfall's behaviour, the location of the material brought from the mountain face, and supports the initial hypothesis of a landslide as the source material for the younger deposits in the valley. We discuss further in-depth caveats on the modelling in the supplementary section.

5.4 Stochastic versus external forcing for aggradation-incision cycles

The alluvial deposits in the Klados catchment are unique compared to other catchments in southern Crete. We have demonstrated that the deposits preserved in the valley are Holocene in age and that following a massive landslide event, the catchment dynamics are best described by rapid and dramatic alternations between valley-wide aggradation and incision. These findings suggest that the emplacement of the landslide deposit altered catchment dynamics, making Klados ultra-sensitive to external forcing. Below, we detail the sequence of events that describe the Holocene evolution of the Klados catchment and the response of the mechanism for rapid alternations between aggradation and incision.

https://doi.org/10.5194/esurf-2021-4
Preprint. Discussion started: 10 February 2021

Combining the relative and absolute chronology ends in the following history for the Holocene topographic evolution of the Klados catchment (Fig. 8). The backfilled paleo-topography preserved beneath the L_1 deposits indicates that the catchment was originally a bedrock-dominated channel similar to the adjacent catchments. Based on this unconformity and the sedimentology of L_1, the bedrock valley was filled with unconsolidated L_1 sediment instantaneously. The sedimentology and distribution of L_1 deposits are most consistent with a landslide following a large rockfall event in the catchment's headwaters. Our interpretation, reinforced by landslide runout modelling, is that the rockfall detached in the headwaters of the catchment, and upon impact with the valley floor partly liquefied and pulverised, sending debris downstream, eventually backfilling the valley up to 100 m locally, as is evidenced by preserved deposits in the high altitudes of the hillslopes surrounding the channel (L_1).

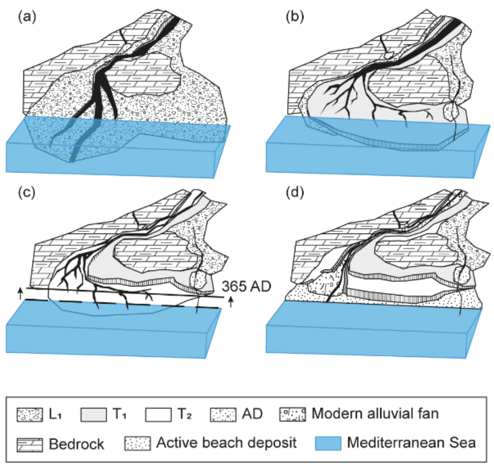

Figure 8: Summary of the evolution of the Holocene deposits at the outlet of the Klados catchment. Prior to the landslide, the valley was likely a sediment-limited, bedrock-dominated catchment similar to its modern neighbours. (a) The landslide filled the valley, which provided tools for the subsequent incision. (b) After having incised nearly to the bedrock, an unknown event caused sediment remobilisation and aggradation of T_1. (c) The earthquake in AD 365 uplifted the coastline by 6 m and triggered new debris flows that eventually formed T_2 and buried the uplifted paleobeach. (d) The modern configuration at the beach with two large inset fans burying the paleobeach.

The landslide debris deposit changed the channel's slope and altered the ratio of sediment supply and transport capacity of the Klados River by introducing vast quantities of highly erodible material throughout the valley. To establish a new equilibrium channel slope, as was needed to transport the newly imposed sediment load, a phase of incision commenced controlled by tool availability and the stream's carrying capability. The incision period was vigorous enough for the channel to cut through the deposit and into bedrock, as shown by exposed bedrock strath terraces in the mid-to-upper reaches of the gorge (Fig. 3b). This channel relaxation period was interrupted by several episodes of valley aggradation and incision that resulted in the construction of the alluvial fill deposits, T_1, T_2, and T_3. The stratigraphy of these deposits suggests that aggradation was initiated by a debris flow, as evidenced by the basal debris flow deposits, implying aggradation was event-triggered.

https://doi.org/10.5194/esurf-2021-4
Preprint. Discussion started: 10 February 2021

Events capable of triggering debris flows and liberating vast quantities of material from L_1 are most likely rare, large earthquakes or large precipitation events. There is not enough evidence to discriminate between these triggering events for the T_1 and T_3 deposits; however, field evidence supports an earthquake origin for T_2. T_2 forms a buttress unconformity with the AD 365 sea-level notch and the uplifted AD 365 beach (Fig. 4i). This evidence suggests that aggradation of T_2 may have initiated when the AD 365 event liberated sediment. This observation provides a critical timeframe for the sequence of deposition.

If we assume that the other large-scale aggradation events resulting in T_1 and the initial landslide depositing L_1 were also caused by ground movement related to earthquake activity, we can provide a very crude estimate of the recurrence interval of large earthquakes in the region. Assuming an early to mid-Holocene age of ~10-5 kyrs for the initial rockfall, three large events (initial landslide and two large aggradation events) took place within the last 5-10 kyrs, suggesting a crude recurrence of about 1.5-3.5 kyrs. This estimate is in good agreement with regional and more local recurrence interval estimates of great earthquakes of 800 to 4500 years (Mouslopoulou et al., 2015; Shaw et al., 2008). Of course, this is a rough estimate resting on many untested assumptions. Nevertheless, it illustrates how catchments that are sensitive to external perturbations can serve as exceptional archives, provided the geochronology and causation between catchment and external events are well constrained and documented.

Our field observations and geochronology support an alluvial fan and terrace formation model with four alternating phases of aggradation and incision over a geologically and geomorphically short duration (i.e., several 1000s of years). These phases are caused by the unsteady liberation of highly erodible landslide deposit material that overwhelmed the catchment and resulted in thick fans and terraces (cf. Maas and Macklin, 2002; Scherler et al., 2016). Potential mechanisms driving the phases of aggradation and incision need to be quasi-instantaneous, and earthquakes and extreme precipitation events are the most likely options. They are capable of liberating large amounts of unconsolidated sediment in a short amount of time. However, the efficiency of erosion and transport depends not solely on the intensity of precipitation but also on the alternating valley floor width. The confinement in the narrow gorge sections might have resulted in random damming and redistribution of material independent of external forcing. The formation and breakage of dams in the narrow bedrock reaches may have been facilitated by the random occurrence of large blocks and fluctuations in surface discharge. These would have influenced river transport capacity and sediment transport or deposition, leading to precipitation-independent incision and aggradation by obstruction. Consequently, we argue that the substantial sediment input changed the aggradation and incision cycles in the Klados River system from those dependent on climate and sediment availability to those dependent on seismicity, hillslope failures, and stochastic events such as hydraulic and sediment damming upstream from narrow bedrock reaches.

https://doi.org/10.5194/esurf-2021-4
Preprint. Discussion started: 10 February 2021

6 Summary and conclusions

The Klados catchment is located in a semi-arid, highly dynamic bedrock landscape and features a set of prominent fill terraces. Our results show that the impressive stratigraphic sequence in the Klados catchment is Holocene in age, and we propose that a rockfall from Volakias Mountain supplied the sediment that led to valley infill by debris flows and the formation of terraces due to incision and alluviation. The occurrence of a rockfall followed by a landslide is supported by the cliff face morphology, sedimentological characteristics of the deposit, and the results from dynamic runout modelling. The debris flow origin of the younger deposits is supported by sedimentological and morphological observations. Possible drivers for aggradation and incision are fluctuations in precipitation, which influenced river transport capacity, the stochastic damming in the narrow bedrock reaches of the valley, and the increased remobilisation of sediment due to seismic ground accelerations. Our Holocene radiocarbon ages reveal that the deposits formed by reworking the landslide material are much younger than previously assumed, and the infilling and subsequent terrace formation by erosion must have followed quickly after one another. At least two remobilisation events are recorded in the structure of the deposits, of which the latter is likely related to the AD 365 earthquake that lifted the beach by 6 m. The radiocarbon ages of the deposits and the close relationships between the units and the AD 365 bioerosional notch reveal that aggradation occurred during the mid-to-late Holocene, and necessarily, the landslide happened before. The initial rockfall in the gorge is likely connected to the seismic activity and the resulting weakening of the bedrock cliff facing the valley. The Klados catchment is an excellent example of how stochastic events can generate river terraces and alluvial fans and how particular river catchments can become hyper-sensitive to external perturbations and thereby offer the potential archiving of these external forces.

7 Author contribution

S.G. and K.W. planned this investigation. S.G., R.O., and E.B. are responsible for mapping and field observations. N.H. assisted with radiocarbon analyses, K.W. provided radiocarbon measurements on terrestrial snails, E.B. modelled the landslide runout, and V.P. advised on structure and sedimentology. E.B. prepared the samples, analysed the results, and wrote the manuscript with contributions by all co-authors.

8 Competing interests

The authors declare that they have no conflict of interest.

9 Acknowledgements

We thank Hellenic Cadastre SA for DEM data. Sincere thanks to Christina Tsimi (NOA) for customising the 5-m digital elevation models for the research area. We thank Jordan Aaron, who provided us with the DAN3D-Flex software, and valuable input on its usage. We thank Jonathan Booth, whose focus on the Klados catchment in his Ph.D. thesis allowed for our accurate digital mapping.

10 References

Aaron, J. and Hungr, O.: Dynamic simulation of the motion of partially-coherent landslides, Eng. Geol., 205, 1–11, doi:10.1016/j.enggeo.2016.02.006, 2016.

Aaron, J., McDougall, S., Moore, J. R., Coe, J. A. and Hungr, O.: The role of initial coherence and path materials in the dynamics of three rock avalanche case histories, Geoenvironmental Disasters, 4(1), 5, doi:10.1186/s40677-017-0070-4, 2017.

Ambraseys, N. N.: Catalogue of Earthquakes 1900-1970, in Earthquakes in the Mediterranean and Middle East: A multidisciplinary study of seismicity up to 1900, pp. 60–795., 2009.

Angelier, J., Lybéris, N., Le Pichon, X., Barrier, E. and Huchon, P.: The tectonic development of the hellenic arc and the sea of crete: A synthesis, Tectonophysics, 86(1–3), doi:10.1016/0040-1951(82)90066-X, 1982.

Benito, G., Macklin, M. G., Zielhofer, C., Jones, A. F. and Machado, M. J.: Holocene flooding and climate change in the Mediterranean, Catena, 130, 13–33, doi:10.1016/j.catena.2014.11.014, 2015.

Blair, T. C. and McPherson, J. G.: Processes and Forms of Alluvial Fans - Geomorphology of Desert Environments, in Geomorphology of Desert Environments, edited by A. J. Parsons and A. D. Abrahams, pp. 413–467, Springer Science & Business Media., 2015.

Booth, J.: The response of Mediterranean steepland coastal catchments to base level and climate change, southwestern Crete, Aberystwyth University., 2010.

Bridgland, D., Maddy, D. and Bates, M.: River terrace sequences: Templates for Quaternary geochronology and marine-terrestrial correlation, J. Quat. Sci., 19(2), 203–218, doi:10.1002/jqs.819, 2004.

Bull, W. B.: Geomorphic responses to climatic change, Oxford University Press, New York., 1991.

Creutzburg, N.: General Geological Map of Greece, Crete Island., 1977.

Dominey-Howes, D., Dawson, A. and Smith, D.: Late Holocene coastal tectonics at Falasarna, western Crete: a sedimentary study, Geol. Soc. London, Spec. Publ., 146(1), 343–352, doi:10.1144/GSL.SP.1999.146.01.20,

https://doi.org/10.5194/esurf-2021-4
Preprint. Discussion started: 10 February 2021

1999.

Dufresne, A.: Rock Avalanche Sedimentology—Recent Progress, in Advancing Culture of Living with Landslides: Volume 2 Advances in Landslide Science, pp. 117–122, Springer International Publishing, Cham., 2017.

ESRI: National Geographic World Map, digital topographic basemap of the world., Natl. Geogr. Esri, DeLorme, NAVTEQ, UNEP-WCMC, USGS, NASA, ESA, METI, NRCAN, GEBCO, NOAA, IPC [online] Available from: https://www.arcgis.com/home/item.html?id=b9b1b422198944fbbd5250b3241691b6#overview (Accessed 21 September 2017), 2011.

Fassoulas, C., Kilias, A. and Mountrakis, D.: Postnappe stacking extension and exhumation of high-pressure/low-temperature rocks in the island of Crete, Greece, Tectonics, 13(1), 127–138, doi:10.1029/93TC01955, 1994.

Ferrier, G. and Pope, R. J. J.: Quantitative mapping of alluvial fan evolution using ground-based reflectance spectroscopy, Geomorphology, 175–176, 14–24, doi:10.1016/j.geomorph.2012.06.013, 2012.

Finnegan, N. J., Schumer, R. and Finnegan, S.: A signature of transience in bedrock river incision rates over timescales of 10 (4) -10 (7) years, Nature, 505(7483), 391–394, doi:10.1038/nature12913, 2014.

Gallen, S. F., Wegmann, K. W., Bohnenstiehl, D. R., Pazzaglia, F. J., Brandon, M. T. and Fassoulas, C.: Active simultaneous uplift and margin-normal extension in a forearc high, Crete, Greece, Earth Planet. Sci. Lett., 398, 11–24, doi:10.1016/j.epsl.2014.04.038, 2014.

Geotag Aeroview: Overview of Crete- Chania, Tripinview [online] Available from: https://www.tripinview.com/presentation?id=64851&lang=en&layer=overview (Accessed 18 January 2018), 2017.

Golden Software, L.: Surfer® from Golden Software, LLC, [online] Available from: www.goldensoftware.com, 2018.

Grämiger, L. M., Moore, J. R., Vockenhuber, C., Aaron, J., Hajdas, I. and Ivy-Ochs, S.: Two early Holocene rock avalanches in the Bernese Alps (Rinderhorn, Switzerland), Geomorphology, 268, 207–221, doi:10.1016/j.geomorph.2016.06.008, 2016.

Grimm, E. C., Maher, L. J. and Nelson, D. M.: The magnitude of error in conventional bulk-sediment radiocarbon dates from central North America, Quat. Res., 72(2), 301–308, doi:10.1016/j.yqres.2009.05.006, 2009.

Haghipour, N., Ausin, B., Usman, M. O., Ishikawa, N., Wacker, L., Welte, C., Ueda, K. and Eglinton, T. I.: Compound-Specific Radiocarbon Analysis by Elemental Analyzer-Accelerator Mass Spectrometry: Precision and Limitations, Anal. Chem., 91(3), 2042–2049, doi:10.1021/acs.analchem.8b04491, 2019.

van Hinsbergen, D. J. J. and Meulenkamp, J. E.: Neogene supradetachment basin development on Crete (Greece) during exhumation of the South Aegean core complex, Basin Res., 18(1), 103–124, doi:10.1111/j.1365-2117.2005.00282.x, 2006.

Hungr, O.: A model for the runout analysis of rapid flow slides, debris flows, and avalanches, Can. Geotech. J., 32(4), 610–623, doi:10.1139/t95-063, 1995.

IUSS Working Group WRB: World Reference Base for Soil Resources 2014, update 2015: International soil classification system for naming soils and creating legends for soil maps., Rome., 2015.

Limaye, A. B. S. and Lamb, M. P.: Numerical model predictions of autogenic fluvial terraces and comparison to

https://doi.org/10.5194/esurf-2021-4
Preprint. Discussion started: 10 February 2021

climate change expectations, J. Geophys. Res. Earth Surf., 121(3), 512–544, doi:10.1002/2014JF003392, 2016.

Maas, G. S. and Macklin, M. G.: The impact of recent climate change on flooding and sediment supply within a Mediterranean mountain catchment, southwestern Crete, Greece, Earth Surf. Process. Landforms, 27(10), 1087–1105, doi:10.1002/esp.398, 2002.

Macklin, M. G. and Woodward, J.: River systems and environmental change, in The Physical Geography of the Mediterranean, edited by J. Woodward, pp. 319–352, Oxford University Press, Chichester., 2009.

Macklin, M. G., Tooth, S., Brewer, P. A., Noble, P. L. and Duller, G. A. T.: Holocene flooding and river development in a Mediterranean steepland catchment: The Anapodaris Gorge, south central Crete, Greece, Glob. Planet. Change, 70(1–4), 35–52, doi:10.1016/j.gloplacha.2009.11.006, 2010.

McClusky, S., Balassanian, S., Barka, A., Demir, C., Ergintav, S., Georgiev, I., Gurkan, O., Hamburger, M., Hurst, K., Kahle, H., Kastens, K., Kekelidze, G., King, R., Kotzev, V., Lenk, O., Mahmoud, S., Mishin, A., Nadariya, M., Ouzounis, A., Paradissis, D., Peter, Y., Prilepin, M., Reilinger, R., Sanli, I., Seeger, H., Tealeb, A., Toksöz, M. N. and Veis, G.: Global Positioning System constraints on plate kinematics and dynamics in the eastern Mediterranean and Caucasus, J. Geophys. Res. Solid Earth, 105(B3), 5695–5719, doi:10.1029/1999JB900351, 2000.

McIntyre, C. P., Wacker, L., Haghipour, N., Blattmann, T. M., Fahrni, S., Usman, M., Eglinton, T. I. and Synal, H.-A.: Online 13C and 14C Gas Measurements by EA-IRMS–AMS at ETH Zürich, Radiocarbon, 59(03), 893–903, doi:10.1017/RDC.2016.68, 2017.

Merritts, D. J., Vincent, K. R. and Wohl, E. E.: Long river profiles, tectonism, and eustasy: A guide to interpreting fluvial terraces, Jounral Geophys. Res., 99(B7), 14031–14050, 1994.

Meulenkamp, J. E., van der Zwaan, G. J. and van Wamel, W. A.: On late Miocene to recent vertical motions in the Cretan segment of the Hellenic arc, Tectonophysics, 234(1–2), 53–72, doi:10.1016/0040-1951(94)90204-6, 1994.

Mouslopoulou, V., Nicol, A., Begg, J., Oncken, O. and Moreno, M.: Clusters of megaearthquakes on upper plate faults control the Eastern Mediterranean hazard, Geophys. Res. Lett., 42(23), 10282–10289, doi:10.1002/2015GL066371, 2015.

Mouslopoulou, V., Begg, J., Fülling, A., Moraetis, D. and Partsinevelos, P.: Distinct phases of eustatic and tectonic forcing for late Quaternary landscape evolution in southwest Crete , Greece, Earth Surf. Dyn., 5, 511–527, 2017.

Nagelisen, J., Moore, J. R., Vockenhuber, C. and Ivy-Ochs, S.: Post-glacial rock avalanches in the Obersee Valley, Glarner Alps, Switzerland, Geomorphology, 238, 94–111, doi:10.1016/j.geomorph.2015.02.031, 2015.

Nash, D. B.: Morphologic dating of degraded normal fault scarps., J. Geol., 88(3), 353–360, doi:10.1086/628513, 1980.

Nemec, W. and Postma, G.: Quaternary alluvial fans in southwestern Crete: sedimentation processes and geomorphic evolution, in Alluvial Sedimentation, edited by M. Marzo and C. Puigdefábregas, pp. 235–276., 1993.

Ott, R. F., Gallen, S. F., Caves Rugenstein, J. K., Ivy-Ochs, S., Helman, D., Fassoulas, C., Vockenhuber, C., Christl, M. and Willett, S. D.: Chemical Versus Mechanical Denudation in Meta-Clastic and Carbonate Bedrock Catchments on Crete, Greece, and Mechanisms for Steep and High Carbonate Topography, J. Geophys. Res. Earth Surf., 124(12), 2943–2961, doi:10.1029/2019JF005142, 2019a.

https://doi.org/10.5194/esurf-2021-4
Preprint. Discussion started: 10 February 2021

Ott, R. F., Gallen, S. F., Wegmann, K. W., Biswas, R. H., Herman, F. and Willett, S. D.: Pleistocene terrace formation, Quaternary rock uplift rates and geodynamics of the Hellenic Subduction Zone revealed from dating of paleoshorelines on Crete, Greece, Earth Planet. Sci. Lett., 525, 115757, doi:10.1016/j.epsl.2019.115757, 2019b.

Pazzaglia, F. J.: Fluvial Terraces, in Treatise on Geomorphology, vol. 9, pp. 379–412, California Academic Press, San Diego, California., 2013.

Pirazzoli, P. A., Thommeret, J., Laborel, J. and Montaggioni, L. F.: Crustal Block Movements from Holocene Shorelines: Crete and Antikythira (Greece), Tectonophysics, 86, 27–43, 1982.

Pirazzoli, P. A., Laborel, J. and Stiros, S. C.: Earthquake clustering in the Eastern Mediterranean during historical times, J. Geophys. Res., 101(B3), 6083–6097, 1996.

Pope, R., Wilkinson, K., Skourtsos, E., Triantaphyllou, M. and Ferrier, G.: Clarifying stages of alluvial fan evolution along the Sfakian piedmont, southern Crete: New evidence from analysis of post-incisive soils and OSL dating, Geomorphology, 94(1–2), 206–225, doi:10.1016/j.geomorph.2007.05.007, 2008.

Pope, R., Candy, I. and Skourtsos, E.: A chronology of alluvial fan response to Late Quaternary sea level and climate change, Crete, Quat. Res. (United States), 86(2), 170–183, doi:10.1016/j.yqres.2016.06.003, 2016.

Reilinger, R., McClusky, S., Vernant, P., Lawrence, S., Ergintav, S., Cakmak, R., Ozener, H., Kadirov, F., Guliev, I., Stepanyan, R., Nadariya, M., Hahubia, G., Mahmoud, S., Sakr, K., ArRajehi, A., Paradissis, D., Al-Aydrus, A., Prilepin, M., Guseva, T., Evren, E., Dmitrotsa, A., Filikov, S. V., Gomez, F., Al-Ghazzi, R. and Karam, G.: GPS constraints on continental deformation in the Africa-Arabia-Eurasia continental collision zone and implications for the dynamics of plate interactions, J. Geophys. Res. Solid Earth, 111(5), doi:10.1029/2005JB004051, 2006.

Rhodes, E. J.: Optically Stimulated Luminescence Dating of Sediments over the Past 200,000 Years, Annu. Rev. Earth Planet. Sci., 39(1), 461–488, doi:10.1146/annurev-earth-040610-133425, 2011.

Robertson, J., Meschis, M., Roberts, G. P., Ganas, A. and Gheorghiu, D. M.: Temporally Constant Quaternary Uplift Rates and Their Relationship With Extensional Upper-Plate Faults in South Crete (Greece), Constrained With 36Cl Cosmogenic Exposure Dating, Tectonics, 38(4), 1189–1222, doi:10.1029/2018TC005410, 2019.

Rothacker, L., Dreves, A., Sirocko, F., Grootes, P. M. and Nadeau, M.-J.: Dating Bulk Sediments from Limnic Deposits Using a Grain Size Approach, in Proceedings of the 21st International Radiocarbon Conference, vol. 55, edited by A. J. T. Jull and C. Hatté, pp. 943–950., 2013.

Ruff, M., Fahrni, S., Gäggeler, H. W., Hajdas, I., Suter, M., Synal, H. A., Szidat, S. and Wacker, L.: On-line radiocarbon measurements of small samples using elemental analyzer and MICADAS gas ion source, Radiocarbon, 52(4), 1645–1656, doi:10.1017/S003382220005637X, 2010.

Scherler, D., Lamb, M. P., Rhodes, E. J. and Avouac, J. P.: Climate-change versus landslide origin of fill terraces in a rapidly eroding bedrock landscape: San Gabriel River, California, Bull. Geol. Soc. Am., 128(7), 1228–1248, doi:10.1130/B31356.1, 2016.

Schumm, S. A.: Geomorphic Thresholds and Complex Response of Drainage Systems, in Fluvial Geomorphology, pp. 299–310, Colorado., 1973.

Schwanghart, W. and Scherler, D.: Short Communication: TopoToolbox 2 - MATLAB-based software for topographic analysis and modeling in Earth surface sciences, Earth Surf. Dyn., 2(1), 1–7, doi:10.5194/esurf-2-1-2014, 2014.

https://doi.org/10.5194/esurf-2021-4
Preprint. Discussion started: 10 February 2021

Earth Surface Dynamics Discussions

Shaw, B., Ambraseys, N. N., England, P. C., Floyd, M. A., Gorman, G. J., Higham, T. F. G., Jackson, J. A., Nocquet, J.-M., Pain, C. C. and Piggott, M. D.: Eastern Mediterranean tectonics and tsunami hazard inferred from the AD 365 earthquake, Nat. Geosci., 1(4), 268–276, doi:10.1038/ngeo151, 2008.

Stiros, S. C.: The AD 365 Crete earthquake and possible seismic clustering during the fourth to sixth centuries AD in the Eastern Mediterranean: A review of historical and archaeological data, J. Struct. Geol., 23(2–3), 545–562, doi:10.1016/S0191-8141(00)00118-8, 2001.

Strasser, T. F., Runnels, C., Wegmann, K., Panagopoulou, E., Mccoy, F., Digregorio, C., Karkanas, P. and Thompson, N.: Dating Palaeolithic sites in southwestern Crete, Greece, J. Quat. Sci., 26(5), 553–560, doi:10.1002/jqs.1482, 2011.

Thorndycraft, V. R. and Benito, G.: Late Holocene fluvial chronology of Spain: The role of climatic variability and human impact, Catena, 66(1–2), 34–41, doi:10.1016/j.catena.2005.07.007, 2006.

USGS: Catastrophic Landslides of the 20th Century - Worldwide, USGS - Landslide Hazards [online] Available from: https://www.usgs.gov/natural-hazards/landslide-hazards/science/catastrophic-landslides-20th-century-worldwide?qt-science_center_objects=0#qt-science_center_objects (Accessed 20 July 2018), 2016.

Wacker, L., Němec, M. and Bourquin, J.: A revolutionary graphitisation system: Fully automated, compact and simple, Nucl. Instruments Methods Phys. Res. Sect. B Beam Interact. with Mater. Atoms, 268(7–8), 931–934, doi:10.1016/j.nimb.2009.10.067, 2010.

Wegmann, K. W.: Tectonic Geomorphology above Mediterranean Subduction Zones: Northeastern Apennines of Italy and Crete, Greece, Lehigh University., 2008.

Wieczorek, G. F., Snyder, J. B., Waitt, R. B., Morrissey, M. M., Uhrhammer, R. A., Harp, E. L., Norris, R. D., Bursik, M. I. and Finewood, L. G.: Unusual July 10, 1996, rock fall at Happy Isles, Yosemite National Park, California, Bull. Geol. Soc. Am., 112(1), 75–85, doi:10.1130/0016-7606(2000)112<75:UJRFAH>2.0.CO;2, 2000.

Zachariasse, W. J., van Hinsbergen, D. J. J. and Fortuin, A. R.: Formation and fragmentation of a late Miocene supradetachment basin in central Crete: Implications for exhumation mechanisms of high-pressure rocks in the Aegean forearc, Basin Res., 23(6), 678–701, doi:10.1111/j.1365-2117.2011.00507.x, 2011.

Zielhofer, C., Faust, D. and Linstädter, J.: Late Pleistocene and Holocene alluvial archives in the Southwestern Mediterranean: Changes in fluvial dynamics and past human response, Quat. Int., 181(1), 39–54, doi:10.1016/j.quaint.2007.09.016, 2008.